

The influence of the R47H *TREM2* variant on microglial exosome profiles

Running title: *TREM2* variant microglial exosomes

Anna Mallach¹, Johan Gobom^{2,3}, Henrik Zetterberg^{2,3,4,5}, John Hardy^{4,5,6,7,8}, Thomas M Piers¹, Selina Wray⁴, Jennifer M Pocock^{1*}

¹Department of Neuroinflammation, UCL Queen Square Institute of Neurology, University College London, WC1N 1PJ, UK

²Department of Psychiatry and Neurochemistry, Institute of Neuroscience and Physiology, University of Gothenburg S-431 80, Mölndal, Sweden

³Clinical Neurochemistry Laboratory, Sahlgrenska University Hospital, S-431 80 Mölndal, Sweden

⁴Department of Neurodegenerative Disease, UCL Queen Square Institute of Neurology, London, WC1N 1PJ, and WC1N 3BG UK

⁵UK Dementia Research Institute at UCL, London WC1E 6BT, UK

⁶Reta Lila Weston Institute, UCL Queen Square Institute of Neurology, 1 Wakefield Street, London WC1N 1PJ, UK

⁷NIHR University College London Hospitals Biomedical Research Centre, London, UK

⁸Institute for Advanced Study, The Hong Kong University of Science and Technology, Hong Kong SAR, China

*corresponding author; j.pocock@ucl.ac.uk

Abstract

Variants in the triggering receptor expressed on myeloid cells 2 (*TREM2*) gene are linked with an increased risk of dementia, in particular the R47H^{het} *TREM2* variant is linked to late-onset Alzheimer's disease. Using human iPSC-derived microglia, we assessed whether variations in the dynamics of exosome secretion, including their components, from these cells might underlie some of this risk. We found exosome size was not altered between common variant controls and R47H^{het} variants, but the amount and constitution of exosomes secreted were different. Exosome quantities were rescued by incubation with an ATP donor or with lipids via a phosphatidylserine *TREM2* ligand. Following a lipopolysaccharide or phagocytic cell stimulus, exosomes from common variant and R47H^{het} microglia were found to contain cytokines, chemokines, APOE and *TREM2*. Differences were observed in the expression of CCL22, IL-1 β and *TREM2* between common variant and R47H^{het} derived exosomes. Furthermore unlike common variant-derived exosomes, R47H^{het} exosomes contained additional proteins linked to negative regulation of transcription and metabolic processes. Subsequent addition of exosomes to stressed neurones showed R47H^{het}-derived exosomes to be less protective. These data have ramifications for the responses of microglia in Alzheimer's disease and may point to further targets for therapeutic intervention.

Keywords (5): Exosomes, Alzheimer's disease, microglia, TREM2

Abbreviations used: AD = Alzheimer's disease, CPZ = chlorpromazine, Cv = common variant, CytoD = Cytochalasin D, DIV = days in vitro, EB = embryoid bodies, ER = endoplasmic reticulum, FACs = fluorescence activated cell sorting, H₂O₂ = hydrogen peroxide, iPSC = induced pluripotent stem cells, iPS-Mg = induced pluripotent stem cell-derived microglia, LC-MS = liquid chromatography mass spectrometry, LPS = lipopolysaccharide, NTA = nanoparticle tracking analysis, PBST = phosphate buffered saline solution with 1% TWEEN-20, PI = propidium iodide, PS⁺ = phosphatidylserine, RA = retinoic acid, SDC = sodium deoxycholate, SN = supernatant, TREM2 = triggering receptor expressed on myeloid cells 2.

Introduction

Alzheimer's disease (AD) is the most common neurodegenerative disease with complex underlying disease mechanisms leading to inflammation in the brain and neuronal death (Minagar *et al.*, 2002; Heneka *et al.*, 2013; Zhang *et al.*, 2013). Genome-wide association studies have linked enhanced risk of developing AD with inflammation, notably the innate immune cells of the brain, microglia (Naj *et al.*, 2011; Guerreiro *et al.*, 2013; Jonsson *et al.*, 2013b). Microglia support neuronal functioning and viability through a range of processes, such as synaptic pruning, production of neurotrophic factors and reacting to threats in the environment (Minagar *et al.*, 2002; Penzes *et al.*, 2011; Parkhurst *et al.*, 2013; Miyamoto *et al.*, 2016). The triggering receptor expressed on myeloid cells-2 (TREM2) is involved in this surveillance function, as mutations in the gene for this receptor have been shown to reduce phagocytosis, migration and response to extracellular stimuli (Ulland *et al.*, 2017; Zhong *et al.*, 2017; Garcia-Reitboeck *et al.*, 2018; Piers *et al.*, 2020). Heterozygous mutations in *TREM2*, such as the R47H^{het} mutation, are associated with AD (Guerreiro *et al.*, 2013; Jonsson *et al.*, 2013), whilst homozygous missense *TREM2* mutations such as T66M cause Nasu-Hakola disease, a rare early-onset dementia with bone cysts (Paloneva *et al.*, 2002; Guerreiro *et al.*, 2013).

Exosomes are small extracellular vesicles ranging from 30-200nm in size (Hooper *et al.*, 2012; Yang *et al.*, 2018; Mathieu *et al.*, 2019), created through endocytosis in multi-vesicular bodies and subsequent fusion and release (Hsu *et al.*, 2010). Microglial exosomes have been shown to fulfil different functions, including supporting neuronal viability and functioning (Antonucci *et al.*, 2012; Gupta and Pulliam, 2014; Asai *et al.*, 2015). Upon activation of microglia with the toll-like receptor 4 agonist, lipopolysaccharide (LPS), subsequently secreted exosomes have been shown to contain inflammatory cytokines (Yang *et al.*, 2018) and in turn, differentially affect neighbouring neurons. Since *TREM2* variants and knock-outs have been shown to have an altered responsiveness to pathogenic stimulation (Ito and Hamerman, 2012) and display an impaired metabolism (Ulland *et al.*, 2017; Piers *et al.*, 2020), this could potentially affect exosomal production and release. We hypothesise that microglia with the AD-associated R47H^{het}*TREM2* variant have an altered exosome secretion and that the exosomes have a differential effect on the viability of neurons. To study this, we used human induced pluripotent stem cells (iPSC) from patients carrying the R47H^{het} mutation, differentiated into functional microglia (iPS-Mg). We analysed the composition of the exosomes and then examined their potential to influence neurones.

Methods

iPS generation and iPS-Mg cells

Ethical permission for this study was obtained from the National Hospital of Neurology and Neurosurgery and the Institute of Neurology joint research ethics committee (study reference 09/H0716/64). R47H^{het} fibroblasts were acquired under a material transfer agreement between University College London and University of California Irvine Alzheimer's Disease Research Centre (UCI ADRC; Professor M Blurton-Jones). Lines from 3 different patients carrying the R47H variant were used, with 8 clones in total being used. For one patient line, only 2 clones were included in the analysis due to chromosome abnormalities in the last clone.

Reprogramming of the R47H^{het} fibroblasts was performed as previously described (Xiang *et al.*, 2018), with plasmids obtained from Addgene (#27077, #27078, #27080). After 7 days in vitro (DIV) nucleofected cultures were transferred to Essential 8 medium (Life Technologies) and colonies were picked after 25-30 DIV. Karyotype analysis was performed by The Doctors Laboratory (London). The iPSC were maintained and passaged in Essential 8 medium. Control lines used in this study were: CTRL1 (kindly provided by Dr Selina Wray, UCL Queen Square Institute of Neurology), BIONi010-C (obtained from EBiSC), SFC840 and SBAD03 (obtained from Stembancc) and KOLF2-C1 (obtained from Sanger Institute, available through EBiSC).

Using previously described protocols, iPS-Mg were generated (Xiang *et al.*, 2018). Briefly, embryoid bodies (EB) were generated and maintained for 5 days in 100 ng/ml ROCK inhibitor, 50 ng/ml VEGF, 50 ng/ml BMP-4 and 20 ng/ml SCF. The EB were collected and transferred to flasks for further differentiation and kept in X-VIVO15 (Lonza) with 100 ng/ml MCSF and 25 ng/ml IL3. After 4-5 weeks of maturation, progenitor cells are collected and plated in iPS-Mg maintenance medium, containing 100 ng/ml IL-34, 25 ng/ml MCSF and 5 ng/ml TGF- β , with the medium being changed every 3-4 days. Two weeks after plating, maturation medium containing 100 ng/ml CX3CL1 and 100 ng/ml CD200 was added to the cells in addition to IL-34, MCSF and TGF- β for another 3 days to achieve final maturation into iPS-Mg, which was confirmed through a custom-designed gene array testing for 28 microglial genes (Xiang *et al.*, 2018).

SH-SY5Y culture

SH-SY5Y cells (a kind gift from Professor R De Silva, UCL Queen Square Institute of Neurology) were maintained and passaged in DMEM (ThermoFisher) containing 15% foetal bovine serum and penicillin/streptomycin (20 units/ml). The cells were differentiated using a previously established protocol (Encinas *et al.*, 2000). After 5 days of retinoic acid treatment (10 μ M), the serum was removed from the medium and 50 ng/ml BDNF (Peprotech) was added for another 7 days. Exosomes were added to the SH-SY5Y neurons after differentiation for 24 h (unless stated differently), with the amount adjusted to total exosomal protein, this was 6 μ g/ml.

Apoptotic neurons were generated from undifferentiated SH-SY5Y through heat-shock for 2 h at 45°C. The effectiveness of this method to induce apoptosis in SH-SY5Y was confirmed through Annexin V FITC (Miltenyi Biotech) /propidium iodide (PI) double-staining as previously shown (Garcia-Reitboeck *et al.*, 2018).

iPS-Mg Exosome collection and extraction

Medium was changed on the iPS-Mg 24 h before the experiment. Following treatment with 100 ng/ml LPS or apoptotic neurons at a ratio of 2:1 apoptotic neurons:microglia for 24 h, the supernatant (SN) from the iPS-Mg was collected and centrifuged for 15 min at 300 g. The SN was then used for extracting the exosomes.

Exosomes were extracted using an ExoQuick-TC kit (System Biosciences) by centrifugation of the supernatant for 30 min at 3 000 g before adding the ExoQuick solution overnight at 4°C. Following two further centrifugations at 1 500 g for 30 and 5 min respectively, the pellets from each step were collected. The final exosomal pellet was either resuspended in Dulbecco's phosphate buffered saline without Ca²⁺/Mg²⁺ (DPBS), pH 7.0-7.3 or RIPA buffer (50 mM Tris-HCl, 150 mM NaCl, 1% SDS, 1% Triton X-100, 1 mM EDTA), freshly supplemented with a protease inhibitor cocktail (Halt protease and phosphatase inhibitor (Thermo Fisher Scientific), depending on downstream applications.

Nanoparticle tracking analysis (NTA)

Exosomes collected from 500 000 iPS-Mg over 24 h collection were diluted in 100 µl PBS and loaded into the recording chamber of a NanoSight LM10 (Malvern Panalytical). The content was recorded twice for 30 sec for each sample. For the human CSF standard (SBI System Biosciences, #EXOP-530A-1), 5.5 µg of exosomes were imaged. Analysis of the amount and size of particles per sample was completed with the NTA version 3.2.

Proteomic analysis

Liquid chromatography mass spectrometry (LC-MS) based proteomic analysis was performed using the TMT10-plex method for quantification (McAlister *et al.*, 2014). Protein samples were reduced, alkylated and subjected to trypsin digestion using a filter-assisted sample preparation method, similar to a previously described protocol (Ostasiewicz *et al.*, 2010). Three samples per condition, 12 in total, were arranged into two TMT 10-plex sets, each containing 2 samples of each condition and one reference sample, consisting of a mixture of all samples. To each 240 µl sample, 12 µl 2 M dithiothreitol were added, and the samples were then incubated for 30 min at 60°C. Urea (8 M, 250 µl) was added, and the samples were loaded on molecular-weight cut-off filters (Nanosep, 30 kDa, Pall). Ultrafiltration was performed by centrifugation at 10 000 g for 10 min at RT. The flow-through was discarded and the filters were washed twice with 200 µl 8 M Urea, passing the liquid through the filter by centrifugation as above. The filters were then washed with 200 µl 0.5 % sodium deoxycholate (SDC), 50 mM triethylammonium bicarbonate (digestion buffer). Alkylation of cysteine disulfides was performed by adding 100 µl 18 mM iodoacetamide in digestion buffer to the filters, and incubating for 20 min at RT in darkness. The liquid was removed by centrifugation and the filters were washed twice with 100 µl digestion buffer. Trypsin (Sequencing grade, modified, Promega) in digestion buffer (14 ng/µl, 70 µl) was added to the filters, followed by incubation at 37°C overnight. An additional 10 µl trypsin aliquot (0.1 µg/µl) was added and the samples were further incubated for another four h. Tryptic peptides were collected by centrifugation. TMT 10-plex reagents (8 µg dissolved in 42 µl acetonitrile) were added to the samples followed by incubation for 1 h at room temperature on a shaker. Hydroxylamine (8 µl, 5%)

were added and the samples were incubated for 15 min to inactivate excess TMT reagent, after which the individually TMT-labelled samples were pooled into two multiplex samples. The samples were acidified by addition of 10% trifluoroacetic acid to pH<2 to precipitate the SDC. The samples were centrifuged at 18 000 *g* for 10 min and the supernatants recovered. The TMT labelled peptides were fractionated by reversed-phase chromatography at basic pH (Batth *et al.* 2014). Briefly, the multiplex samples were re-dissolved in 16 μ l 2 % AcN, 5 mM ammonium hydroxide and loaded on an Ultimate 3000 HPLC system (Thermo Fisher). Offline peptide separation was performed over an XBridge BEH130 C18 3.5 μ m, 2.1 mm x 250 mm analytical column at a flow of 100 μ l/min, using a linear gradient and collecting 1 fraction/min for 72 min. Collected fractions were then concentrated to 12 fractions, which were dried by vacuum centrifugation.

For LC-MS, samples were dissolved in 6 μ l of 0.1% TFA and analyzed by LC-MS on nano-HPLC instrument (Ultimate 3000 RSLC nano, Thermo Scientific) fitted with a 75 μ m x 2 cm trap column (PepMap C18, Thermo scientific) and a 75 μ m x 50 cm C18 column (PepMap C18, Thermo scientific), coupled to a Fusion Tribrid mass spectrometer (Thermo scientific). Following 10 min sample loading onto the trap, separation was performed using the following gradient between 0.1% formic acid (Buffer A) and 84% acetonitrile (Buffer B): t=10 (min), 0% B; t=105, %B=40; t=112, %B=99. The mass spectrometer was operated in the positive ion mode, with the following settings: resolution 120 000; m/z range 350-1 400; max injection time 50 ms; AGC target 4e5. Data-dependent acquisition was used to record up to 10 consecutive fragment ion spectra (MS2) per full scan spectrum, selecting precursor ions with charge states 2-7 in decreasing order of intensity, and using 15 s dynamic exclusion. The isolation window was set to 1.2 m/z. The instrument settings for the MS2 scans were: resolution 50 000; fixed first mass m/z 110; max injection time 86 ms; AGC target 5e4.

The LC-MS data were processed using the software Proteome Discoverer 2.3 (Thermo). Protein identification was performed using the Mascot software (Matrix Science), searching the human subset of SwissProt, with the following settings: cleavage enzyme: trypsin; precursor mass tolerance: 15 ppm; fragment mass tolerance: 0.05 Da; static modifications: TMT10-plex; dynamic modifications: phosphorylation. Percolator scoring was used, and validation was performed using the target-decoy approach, using 1% FDR as cut-off for peptide identification. Protein identifications were accepted that had at least one matching peptide.

Microglial gene array

A custom gene array based on published microglial expression data (Butovsky *et al.*, 2014; Muffat *et al.*, 2015; Abud *et al.*, 2017; Haenseler *et al.*, 2017) was used to confirm a microglial signature in our iPS-Mg cultures (TaqMan Array Plate 32 plus Candidate Endogenous Control Genes; Thermo Fisher Scientific, see Table 1), as previously described (Xiang *et al.*, 2018). The heatmap was generated through MATLAB.

Table 1 Microglial gene signature primer details:

Gene name	Primer ID
18 s rRNA	Hs99999901_s1
GAPDH	Hs99999905_m1
HPRT	Hs99999909_m1
GUSB	Hs99999908_m1
APOE	Hs00171168_m1
C1QA	Hs00706358_s1
C1QB	Hs00608019_m1
ITGAM	Hs00167304_m1
CSF1R	Hs00911250_m1
CX3CR1	Hs01922583_s1
GAS6	Hs01090305_m1
GPR34	Hs00271105_s1
AIF1	Hs00610419_g1
MERTK	Hs01031979_m1
OLFML3	Hs01113293_g1
PROS1	Hs00165590_m1
SALL1	Hs01548765_m1
SLCO2B1	Hs01030343_m1
TGFBR1	Hs00610320_m1
TMEM119	Hs01938722_u1
TREM2	Hs00219132_m1
BIN1	Hs00184913_m1
CD33	Hs01076282_g1
SPI1	Hs02786711_m1
HEXB	Hs01077594_m1
ITM2B	Hs00222753_m1
C3	Hs00163811_m1
A2M	Hs00929971_m1
C1QC	Hs00757779_m1
RGS1	Hs01023772_m1
FTL	Hs00830226_gH
P2RY12	Hs01881698_s1

Immunoblotting

For the detection of exosomal CD63, exosomal lysate was deglycosylated using a PNGase kit (New England Biolabs), following manufacturer's instructions. For all other exosomal markers, the exosomal lysates were not deglycosylated. Exosomal pellets or iPS-Mg cells were lysed in RIPA buffer as described above. Cell samples were cleared of nuclear material and cell fragments by centrifugation at 15 000 *g* for 15 min. The cell lysate was denatured using sample buffer and separated by SDS-PAGE. Proteins were transferred onto nitrocellulose membranes and blocked with 5% milk in phosphate buffered saline solution with 1% TWEEN-20 (PBST). For exosomal blots, positive controls consisted of purified exosomes from human serum or Jurkat T lymphocytes (System Biosciences)

Primary antibodies (see Table 2) below were incubated with the blots overnight at 4°C, with the appropriate secondary fluorescently conjugated antibody incubated at 1:5 000 for 1 h at RT.

Table 2 List of antibodies used:

Antibody	Concentration	Diluted In	Company
CD63	1:1000	5% milk	Abcam
ALIX	1:1000	5% milk	Cell Signalling Technologies
CD9	1:1000	5% milk	System Biosciences
CD81	1:1000	5% milk	System Biosciences
Calnexin	1:1000	1% BSA	Santa Cruz
β-actin	1:10,000	1% milk	Thermofisher

Exosomal uptake

Uptake of exosomes into SH-SY5Y cells was assessed with fluorescence activated cell sorting (FACs). The exosomes were labelled with cell Vybrant Dil (Thermofisher) at a dilution of 1:200 at 37°C for 1 h. The excess dye was removed using 3 kDa NMWL columns (Amicon), by centrifuging excess dye out for 20 min at 14 000 *g*. To control for any remaining unbound Dil present after centrifugation, PBS alone was incubated with the dye as well and used as a negative control. The labelled exosomes were then added to SH-SY5Y for 2 h, before the cells were detached using PBS and analysed by FACS. As a negative control, some SH-SY5Y were pre-treated with cytochalasin D (CytoD, 10 μM), chlorpromazine (CPZ, 5 μg/ml) or genistein (200 μM) to inhibit phagocytosis, for 30 min before exposure to labelled exosomes. The data were analysed using Flowing Software 2.

To further visualize exosomal uptake, exosomes were stained with cell Vybrant DiO (Thermofisher) at a dilution of 1:200 at 37°C for 1 h, before excess dye was removed using 3 kDa NMWL columns (Amicon), as described above. The SH-SY5Y were labelled with BioTracker 555 Orange Cytoplasmic Membrane Dye (Merck Millipore) at 2 μg/ml for 10 min. The cytoplasmic membrane labelling was carried out either before exosome incubation in the 1 h condition or after exosome incubation in the 24 h condition. Nuclei were stained with DAPI before being mounted and imaged with a Zeiss LSM710 confocal microscope.

Cell death FACs

To analyse the ability of exosomes to modify neuronal death, we treated SH-SY5Y cells with hydrogen peroxide (H_2O_2 , 100 μM) for 24 h with or without iPS-Mg exosomes. Subsequently SH-SY5Y cells were labelled with propidium iodide (PI, 5 $\mu\text{g}/\text{ml}$) for 15 min before cell death was analysed by FACs. Controls consisted of unstained cells or cells boiled at 95°C for 1 h prior to PI labelling. Data were analysed using Flowing Software 2. and plotted as % of cells in H2 region/total number of cells.

ATP analysis

ATP levels were determined in the iPS-Mg using a commercially available ATP kit (#A22066, Thermo Fisher Scientific). The cells were plated in black walled, glass-bottomed 96-well plates. The iPS-Mg were treated with either apoptotic neurons (2:1 apoptotic neurons: iPS-Mg) or cyclocreatine (10 mM) for 24 h before they were lysed in cell lysis reagent (#1715747, Boehringer Mannheim) and centrifuged at 1,000g for 1 min. Then, 10 μl of sample supernatant or ATP standard was added to 100 μl of the ATP reaction mix, after the background luminescence was read. Luminescence was recorded on a Tecan 10M plate reader. Data were normalised to ATP standard curves and then to the protein concentration of the sample determined by BCA assay.

Statistical Analysis

The results were represented as mean of at least three separate experiments with internal replicates of at least three \pm SEM with a p value of 0.05 or below considered statistical significant. The results were analysed using Prism Software version 5. Analysis was performed on pooled control lines and pooled R47H^{het} cell lines.

With regard to the LC-MS data, the relative abundances, normalised to the reference sample, were analysed using MATLAB and tested for normality and the potential influence of the different experimental runs. Following from this quality control, the abundances were normalised to the individual reference sample for each experimental run, accounting for the overall different number of proteins detected in the samples. In addition to this, for further analysis, the abundance ratios were \log_{10} -transformed to generate a normal distribution, allowing for standard statistical tests to be performed on the data. The results from the data base search were analysed using MATLAB. Analysis of the functional effect of the different proteins was conducted using FunRich and STRING.

Power calculations for exosomal size differences as measured through NTA (Fig 1D) were performed in line with Yang et al., 2018 and statistics were performed using the D90 measurement (calculated = 9). We include $n=10$ for the Cv and $n=11$ for the TREM2 R47H^{het} and therefore achieve the necessary power required to state that based on the D90 measurement no difference is observed.

Data availability

All data are available upon request. All data points are shown on graphs.

Results

Exosome characterisation

To confirm that the particles in the exosomal fraction were indeed exosomes, we assessed whether they displayed common exosomal characteristics. Classical exosomal markers, such as CD63, CD9, ALIX, CD81, HSP70, TSG101 and Flotillin-1 (Hooper *et al.*, 2012; Witwer *et al.*, 2013; Frohlich *et al.*, 2014; Mehdiani *et al.*, 2015; Schiera *et al.*, 2015; Horibe *et al.*, 2018; Chen *et al.*, 2019) were all found to be expressed in the iPS-Mg exosomal fraction of both common variant (Cv) and R47H^{het} derived exosomes (**Fig 1A and Supplementary Fig 1C**). Calnexin, an endoplasmic reticulum (ER) marker, was absent from the exosomal fraction, but shown to be present in the cell lysate (**Fig 1B**) confirming the absence of apoptotic bodies from the exosomal fraction (Lötvall *et al.*, 2014).

The size distribution of the particles as measured through NTA was similar in both Cv and R47H^{het} variants and comparative in size with a human CSF exosome standard (**Fig 1C and 1D**). The average size of the particles was not significantly differently from each other (**Fig 1D**). This was further confirmed by the D90 measurement, again showing no statistical size difference between the Cv and R47H^{het} exosomes (**Supplementary Fig 1B**). These results confirm that the particles found in the iPS-Mg exosomal fraction are indeed exosomal and that they can be extracted reliably from iPS-Mg with *TREM2* variants.

Exosome secretion

As exosome secretion is dependent on interactions with the cytoskeleton and energy availability within the cells (Hoshino *et al.*, 2013; Zou *et al.*, 2019), we investigated the exosome secretion concentration in iPS-Mg carrying the R47H^{het} *TREM2* variant, as it has been shown that these cells have deficits in both their cytoskeleton and metabolic fitness (Takahashi *et al.*, 2005; Ulland *et al.*, 2017; Piers *et al.*, 2020). Measurements by NTA indicated that exosomes were enriched following purification (Video 1) but not present in cell medium alone (Video 2). Further NTA measurements indicated that the concentration of exosomal particles secreted over 24 h from the R47H^{het} expressing iPS-Mg compared with Cv was significantly different (**Fig 1E**). Subsequent analysis of exosomal CD63, a classical marker of exosomes and an approximation of exosomal number, was significantly decreased (**Fig 1F**).

As extracellular stimuli, such as inflammatory signals, can influence the profile of secreted exosomes, both in their size and amount (Qu *et al.*, 2007; Yang *et al.*, 2018), we investigated the amount of exosome secretion following activation of iPS-Mg with 100 ng/ml LPS for 24 h. As we found deficits in exosome secretion in the *TREM2* variant (**Fig 1F**), we also activated the *TREM2*-DAP12 pathway through the addition of apoptotic neurons, which express the *TREM2* ligand phosphatidylserine (PS⁺) on their surface (Wang *et al.*, 2015; Garcia-Reitboeck *et al.*, 2018; Shirotani *et al.*, 2019) and used exosomal CD63 as a readout of exosomal production.

CD63 expression was unchanged in exosomes from Cv or R47H^{het} iPS-Mg with LPS or apoptotic neuron treatment (but was significantly lower in unstimulated and LPS stimulated R47H^{het}-derived exosomes **Fig 2A and B**). Apoptotic neuron-treatment increased exosome secretion from R47H^{het} iPS-Mg (**Fig 2A and B**), whilst Cv exosome secretion was not affected. Apoptotic neurons have been shown

to supply iPS-Mg with additional energy (Cosker *et al.*, 2020), possibly by providing additional energy via lipid catabolism (Nadjar, 2018), rescuing the energy deficit of R47H^{het} iPS-Mg previously reported (Piers *et al.*, 2020). Based on this, we tested whether the increase in exosome secretion from R47H^{het} following exposure to apoptotic neurons was due to an increase in energy supply. Thus, iPS-Mg were treated with 10 mM cyclocreatine for 24 h, which acts as an ATP supply fuelling oxidative phosphorylation rather than glycolysis, which we have shown to be deficient in *TREM2* variant iPS-Mg (Piers *et al.*, 2020). Again, an increase in exosomal CD63 expression was observed in the R47H^{het} exosomes (**Fig 2C** and **D**), whilst there was no significant difference in Cv, suggesting that the reported energy deficit also underlies the reduced secretion of exosomes in the R47H^{het} iPS-Mg. Furthermore analyses of ATP content revealed that there was a significantly lower level of ATP in R47H^{het} cells relative to Cv, and this was increased to Cv levels by prior exposure to PS⁺ cells or cyclocreatine (**Supplementary Fig 2A**).

Exosome content by MS analysis

LC-MS performed on exosomes extracted from iPS-Mg revealed over 70% of the proteins detected have been previously linked to exosomal proteins (**Fig 3A**) and furthermore, by virtue of their cellular compartment of origin, these proteins were found in exosomes, (**Fig 3B**), providing additional support that the extracted particles from iPS-Mg were exosomes.

Analysis of baseline differences between exosomes secreted from Cv and R47H^{het} iPS-Mg by volcano plot revealed nine proteins with higher abundance in R47H^{het} iPS-Mg (ratio > 2, $p < 0.05$). (**Fig 3C**, and **Supplementary Fig 2C**). STRING analyses revealed that some of these proteins are involved in the negative regulation of transcription and metabolic processes (**Fig 3D**).

Analysis of microglial gene signature was assessed in all lines studied using a custom gene array based on previously published expression data (Xiang *et al.*, 2018). Lines from both *TREM2* genotypes used in this study cluster strongly together with only one outlier observed clustering more closely with human macrophages (**Fig 3E**). These data suggest differences observed in exosomal content between genotypes is not due to gross microglial gene signature differences at basal.

Exosome content following LPS or apoptotic cell stimulation

We investigated changes in the relative expression of exosomal proteins following treatment of iPS-Mg with LPS, as previous research has suggested changes in exosomal proteins occur following activation of microglia (Yang *et al.*, 2018). Volcano plots of proteomic data showed that several proteins differ in abundance in exosomes derived from Cv iPS-Mg and R47H^{het} iPS-Mg with and without stimulation with LPS (**Fig 4A** and **4B** respectively). Following activation with LPS, the content of the iPS-Mg exosomes changed significantly to include increased secretion of cytokines in both Cv and R47H^{het} *TREM2* variants, such as TRAF1, (**Fig 4C**), whilst others such as C1QA and APOE showed a significant reduction in exosomes from LPS-treated Cv and R47H^{het} iPS-Mg. *TREM2* was not significantly reduced in exosomes from Cv but was from R47H^{het} exosomes (**Fig 4C**).

Volcano plots of proteomic data from Cv or R47H^{het} derived exosomes exposed to apoptotic neurons revealed differences in abundance (**Fig 5A** and **5B**). Furthermore CCL22 was significantly reduced in

R47H^{het} exosomes compared with Cv following stimulation with apoptotic neurons (**Fig 5C**). Furthermore a significant number of proteins were not increased in R47H^{het} derived exosomes compared with Cv following exposure of iPS-Mg to apoptotic neurons (**Fig 6**).

Uptake of iPS-Mg exosomes into neurons

As microglia exosomes have been shown to affect neuronal functioning (Antonucci *et al.*, 2012; Chen *et al.*, 2019) we determined whether iPS-Mg-derived exosomes from Cv or R47H^{het} cells were taken up into neurons (**Fig 7**). Uptake of the exosomes was verified both through confocal microscopy, showing DiO labelled exosomal particles inside the neurons within 1 h of incubation and 24 h (**Fig 7B**). This was also quantified by FACs, showing a significant uptake of Dil labelled exosomes into the neurons after 2 h in comparison with unstained cells (**Fig 7C and D**). No significant difference was observed in the level of uptake of exosomes from Cv or R47H^{het} iPS-Mg, albeit that the R47H^{het} exosomes appeared to be taken up at slightly lower levels. As a negative control, exosome-free saline solution was incubated with label to control for any carry-over of Vybrant dye, however this appeared not to be a confounding factor (**Fig 7D**). Uptake could be inhibited by CPZ or genistein, but not cytochalasin D (**Fig 6Cii**).

Based on our finding of changes in exosome content in Cv and R47H^{het} exosomes (**Fig 4, 5 and 6**), the effect of exosomes from either Cv or R47H^{het} iPS-Mg on neuronal viability was assessed. Following incubation of exosomes with differentiated SH-SY5Y (see **Supplementary Fig 3** for SH-SY5Y differentiation), no significant differences in the levels of neuronal death were observed after addition of Cv or R47H^{het} exosomes derived from non-treated iPS-Mg (**Fig 8A and 8B**).

Previous research has shown that the protective functions of glial exosomes are more easily revealed when the SH-SY5Y were subjected to H₂O₂-induced cell stress (Pascua-Maestro *et al.*, 2019). Based on this, the ability of exosomes from iPS-Mg to rescue SH-SY5Y neurons from H₂O₂-induced cell death was investigated (**Fig 8C and D**). H₂O₂ increased neuronal death significantly (**Fig 8D**). However, the addition of Cv iPS-Mg-derived exosomes protected SH-SY5Y neurons from H₂O₂-induced death as there was no significant difference between the levels of death in non-treated neurons compared with those treated with Cv exosomes and H₂O₂ indicating a protective effect of Cv-derived exosomes (**Fig 8D**). Conversely, the level of death in neurons treated with H₂O₂ plus exosomes from R47H^{het} iPS-Mg was no different from neurons exposed solely to H₂O₂, indicating that these exosomes were not protective (**Fig 8D**).

Discussion

We were able to reliably extract exosomes from iPS-Mg, the exosomes showed a range of common exosomal markers, and were also devoid of markers which might indicate contamination from different cellular components, such as ER (**Fig 1B**). The average size of the exosomes from cells with or without the R47H^{het} mutation was approximately 150 nm, and a comparison of the size of exosomes from Cv with R47H^{het} indicated that they were not significantly different (**Fig 1D and Supplementary Fig 1B**), suggesting that the R47H^{het} variant does not affect exosome size. Our findings also suggest that the particles as analysed by NTA were potentially larger than those reported elsewhere (Witwer *et al.*, 2013), but in part this can be explained by the measuring technique we employed, as even the CSF

exosome standard was measured to be around the same size as the iPS-Mg derived exosomes (**Fig 1D**). Due to the size of the NTA chamber, during imaging, many particles are out of focus and could skew the average size measured. The R47H^{het} variant appeared to influence exosome number (**Fig 1E**), which was also reflected in the decrease in exosomal CD63 (**Fig 1F**). This could be due to the metabolic deficit in microglia with this variant (Ulland *et al.*, 2017; Piers *et al.*, 2020), as supplying the cells with additional lipids in the form of apoptotic cells was able to alter this to control levels for the protein we tested as indeed did cyclocreatine, generating ATP in the cells (Kurosawa *et al.*, 2012).

In addition to influencing exosome secretion, the R47H^{het} variant altered the packaging of proteins into exosomes, as shown through proteomic analysis with nine proteins increasingly packaged into exosomes from R47H^{het} iPS-Mg which were found to be involved in negative regulation of metabolic processes (**Fig 3C, Fig 3D and Supplementary Fig 2B**). In a recent study, one of the most altered AD protein co-expression modules was linked to sugar metabolism in glia such as microglia (Johnson *et al.*, 2020). Our data suggest that exosome signalling for metabolism is thus likely to be decreased in R47H^{het} iPS-Mg.

Whether these proteins are present in R47H^{het} exosomes because of the metabolic deficits present in the microglia (Ulland *et al.*, 2017; Piers *et al.*, 2020) is not yet known. However, our study confirms previous research that exosomes from LPS-activated microglia contain more inflammatory cytokines (Yang *et al.*, 2018), although we also found that TREM2 was present in exosomes but also decreased following LPS stimulation, and significantly so in R47H^{het} derived exosomes (**Fig 4C**). There were also differences in the proteins present in exosomes from Cv versus R47H^{het} iPS-Mg, and in particular, a number of proteins were not increased in the latter after exposure to apoptotic cells. This suggests that whilst some proteins can be increased by a TREM2 ligand in Cv, in the R47H^{het} iPS-Mg, this is not the case.

Whilst full transcriptomic analysis of the iPS-Mg lines used in this study may go further to identify if there were significant differences in the underlying TREM2 genotypes that could contribute to exosomal content variance, the microglial gene signature array performed here suggests limited differences between the genotypes (**Fig 3E**). Strong clustering between all the lines was observed (with the exception of one potential outlier repeat), suggesting that the TREM2 genotypes do not differ significantly at the microglial signature level. This observation means differences in exosomal content were not likely to be due to differences in the underlying basal microglia signature of the TREM2 variants.

Exosomes can be taken up through a range of different routes into recipient cells (Mulcahy *et al.*, 2014; Schneider *et al.*, 2017; Horibe *et al.*, 2018). We did not find exosome uptake into SH-SY5Y neurons to be inhibited by CytoD, which mainly inhibits phagocytosis and macropinocytosis (Kuhn *et al.*, 2014) through inhibition of actin polymerization, but other uptake mechanisms into SH-SY5Y cells such as membrane fusion and lipid raft-mediated endocytosis are still available for the exosomal cell entry, possibly explaining why exosomal uptake into SH-SY5Y was not blocked. CPZ, an inhibitor of clathrin-mediated endocytosis (Liu *et al.*, 2007; Kuhn *et al.*, 2014; Wesén *et al.*, 2017) or genistein, an inhibitor of caveolin-mediated endocytosis (Horibe *et al.*, 2018), did inhibit uptake however.

Since the same amount of exosomal protein from Cv or R47H^{het} iPS-Mg was added to the neurons and no significant differences were observed in uptake, this suggests that the actual composition and content of R47H^{het} exosomes influences neuronal functioning. When we compared whether the exosomes from either Cv or R47H^{het} affected baseline neuronal viability (**Fig 8A and B**), there was no difference, suggesting that the composition of exosomes from unstimulated iPS-Mg does not in itself influence neuronal viability over the time course of our experiments. However exosomes from Cv were protective against an H₂O₂ stress whilst those from R47H^{het} iPS-Mg were not (**Fig 8C and D**); this may be due to our finding of negative regulators of metabolism being preferentially packaged into R47H^{het} exosomes. It was interesting that exosomes contained TREM2, present in exosomes from Cv and R47H iPS-Mg, although we do not know as yet if this is the full length protein. It has recently been reported that TREM2 is present in exosomes in serum and that these exosomes may transport TREM2 into the brain (Raha-Chowdhury et al., 2018). We show here that exosomes were taken up in neurons, the ramifications of which would need to be further investigated.

In this study, we have shown that exosomes can be reliably extracted from human iPS-Mg expressing *TREM2* variants and that disease-associated *TREM2* variants secrete less exosomes compared with Cv, potentially due to the reported metabolic deficits. Differences in exosomal protein content between the Cv and R47H^{het} iPS-Mg may influence the ability of neurons to protect themselves against H₂O₂ induced stress or other stresses. These differences may influence the ability of human microglia to protect neurons in Alzheimer's disease if the microglia express the R47H^{het} variant.

Acknowledgements

We would like to thank the patients and their families for their participation in this research project; Prof M Blurton-Jones School of Biological Sciences, University of California for providing us with R47H^{het} expressing fibroblasts, and Prof R de Silva, Queen Square Institute of Neurology, UCL, for providing us with SH-SY5Y cells. We would also like to thank the Core Facility for Proteomics at the University of Gothenburg for advice on sample preparation.

Funding

A Mallach was supported by the Biotechnology and Biological Sciences Research Council [grant number BB/M009513/1]. TM Piers was supported by funding to JM Pocock and J Hardy from the Innovative Medicines Initiative 2 Joint Undertaking grant agreement No 115976. This Joint Undertaking receives support from the European Union's Horizon 2020 research and innovation program and EFPIA. H Zetterberg is a Wallenberg Scholar supported by grants from the Swedish Research Council (#2018-02532), the European Research Council (#681712), the Swedish state under the agreement between the Swedish government and the County Councils, the ALF-agreement (#ALFGBG-720931), the Alzheimer Drug Discovery Foundation (ADDF), USA (#201809-2016862), and the UK Dementia Research Institute at UCL. S Wray is supported by an Alzheimer's Research UK Senior Research Fellowship (ARUK-SRF2016B-2) and the National Institute for Health Research University College London Hospitals Biomedical Research Centre.

Competing interests

H Zetterberg has served at scientific advisory boards for Denali, Roche Diagnostics, Wave, Samumed and CogRx, has given lectures in symposia sponsored by Fujirebio, Alzecure and Biogen, and is a co-founder of Brain Biomarker Solutions in Gothenburg AB (BBS), which is a part of the GU Ventures Incubator Program (outside submitted work). The other authors declare that they have no conflict of interest.

References

- Abud, E. M. *et al.* (2017) 'iPSC-Derived Human Microglia-like Cells to Study Neurological Diseases', *Neuron*. Elsevier Inc., 94(2), pp. 278-293.e9. doi: 10.1016/j.neuron.2017.03.042.
- Antonucci, F. *et al.* (2012) 'Microvesicles released from microglia stimulate synaptic activity via enhanced sphingolipid metabolism', *The EMBO Journal*. Nature Publishing Group, 31(5), pp. 1231–1240. doi: 10.1038/emboj.2011.489.
- Asai, H. *et al.* (2015) 'Depletion of microglia and inhibition of exosome synthesis halt tau propagation', *Nature Neuroscience*. Nature Publishing Group, 18(11), pp. 1584–1593. doi: 10.1038/nn.4132.
- Butovsky, O. *et al.* (2014) 'Identification of a Unique TGF- β Dependent Molecular and Functional Signature in Microglia', *Nat Neurosci*, 17(1), pp. 131–143. doi: 10.1038/nn.3599. Identification.
- Chen, X. *et al.* (2019) 'A20 protects neuronal apoptosis stimulated by lipopolysaccharide-induced microglial exosomes', *Neuroscience Letters*. Elsevier, 712(January), p. 134480. doi: 10.1016/j.neulet.2019.134480.
- Choi, D. S. *et al.* (2013) 'Proteomics, transcriptomics and lipidomics of exosomes and ectosomes', *Proteomics*, 13(10–11), pp. 1554–1571. doi: 10.1002/pmic.201200329.
- Cosker, K. *et al.* (2020) 'Microglial signalling pathway deficits associated with the R47H TREM2 variant linked to AD indicate inability to activate inflammasome', *Biorxiv*.
- Encinas, M. *et al.* (2000) 'Sequential Treatment of SH-SY5Y Cells with Retinoic Acid and Brain-Derived Neurotrophic Factor Gives Rise to Fully Differentiated, Neurotrophic Factor-Dependent, Human Neuron-Like Cells'. doi: 10.1046/j.1471-4159.2000.0750991.x.
- Frohlich, D. *et al.* (2014) 'Multifaceted effects of oligodendroglial exosomes on neurons: impact on neuronal firing rate, signal transduction and gene regulation', *Philosophical Transactions of the Royal Society B: Biological Sciences*, 369(1652), pp. 20130510–20130510. doi: 10.1098/rstb.2013.0510.
- Garcia-Reitboeck, P. *et al.* (2018) 'Human Induced Pluripotent Stem Cell-Derived Microglia-Like Cells Harboring TREM2 Missense Mutations Show Specific Deficits in Phagocytosis', *Cell Reports*. Elsevier Company., 24(9), pp. 2300–2311. doi: 10.1016/j.celrep.2018.07.094.
- Guerreiro, R. *et al.* (2013) 'TREM-2 variants in AD', 368(2), pp. 117–127. doi: 10.1056/NEJMoa1211851. TREM2.
- Gupta, A. and Pulliam, L. (2014) 'Exosomes as mediators of neuroinflammation', *Journal of Neuroinflammation*, 11(1), p. 68. doi: 10.1186/1742-2094-11-68.

- Haenseler, W. *et al.* (2017) 'A Highly Efficient Human Pluripotent Stem Cell Microglia Model Displays a Neuronal-Co-culture-Specific Expression Profile and Inflammatory Response', *Stem Cell Reports*.
- Heneka, M. T. *et al.* (2013) 'NLRP3 is activated in Alzheimer's disease and contributes to pathology in APP/PS1 mice.', *Nature*. England, 493(7434), pp. 674–678. doi: 10.1038/nature11729.
- Hooper, C. *et al.* (2012) 'Wnt3a induces exosome secretion from primary cultured rat microglia', *BMC Neuroscience*, 13(1), p. 144. doi: 10.1186/1471-2202-13-144.
- Horibe, S. *et al.* (2018) 'Mechanism of recipient cell-dependent differences in exosome uptake', *BMC Cancer*. BMC Cancer, 18(1), pp. 1–9. doi: 10.1186/s12885-017-3958-1.
- Hoshino, D. *et al.* (2013) 'Exosome secretion is enhanced by invadopodia and drives invasive behavior', *Cell Reports*. The Authors, 5(5), pp. 1159–1168. doi: 10.1016/j.celrep.2013.10.050.
- Hsu, C. *et al.* (2010) 'Regulation of exosome secretion by Rab35 and its GTPase-activating proteins TBC1D10A–C', *The Journal of Cell Biology*, 189(2), pp. 223 LP – 232. Available at: <http://jcb.rupress.org/content/189/2/223.abstract>.
- Ito, H. and Hamerman, J. (2012) 'TREM-2, triggering receptor expressed on myeloid cell-2 negatively regulates TLR responses in dendritic cells', 193(1), pp. 118–125. doi: 10.1016/j.jneumeth.2010.08.011. Autogenic.
- Johnson, E. C. B. *et al.* (2020) 'Large-scale proteomic analysis of Alzheimer's disease brain and cerebrospinal fluid reveals early changes in energy metabolism associated with microglia and astrocyte activation', *Nature Medicine*. doi: 10.1038/s41591-020-0815-6.
- Jonsson, T. *et al.* (2013a) 'Variant of TREM2 associated with the risk of AD', *New England Journal of Medicine*, 368(2), pp. 107–116. doi: 10.1056/NEJMoa1211103. Variant.
- Jonsson, T. *et al.* (2013b) 'Variant of *TREM2* Associated with the Risk of Alzheimer's Disease', *New England Journal of Medicine*, 368(2), pp. 107–116. doi: 10.1056/NEJMoa1211103.
- Kuhn, D. A. *et al.* (2014) 'Different endocytotic uptake mechanisms for nanoparticles in epithelial cells and macrophages', *Beilstein Journal of Nanotechnology*, 5(1), pp. 1625–1636. doi: 10.3762/bjnano.5.174.
- Kurosawa, Y. *et al.* (2012) 'Cyclocreatine treatment improves cognition in mice with creatine transporter deficiency', *Journal of Clinical Investigation*, 122(8), pp. 2837–2846. doi: 10.1172/JCI59373.
- Liu, Y. *et al.* (2007) 'Mechanistic studies of a peptidic GRP78 ligand for cancer cell-specific drug delivery', *Molecular Pharmaceutics*, 4(3), pp. 435–447. doi: 10.1021/mp060122j.
- Lötvall, J. *et al.* (2014) 'Minimal experimental requirements for definition of extracellular vesicles and their functions: A position statement from the International Society for Extracellular Vesicles', *Journal of Extracellular Vesicles*, 3(1), pp. 1–6. doi: 10.3402/jev.v3.26913.
- Mathieu, M. *et al.* (2019) 'Specificities of secretion and uptake of exosomes and other extracellular

vesicles for cell-to-cell communication', *Nature Cell Biology*. Springer US, 21(1), pp. 9–17. doi: 10.1038/s41556-018-0250-9.

McAlister, G. C. *et al.* (2014) 'MultiNotch MS3 enables accurate, sensitive, and multiplexed detection of differential expression across cancer cell line proteomes', *Analytical Chemistry*, 86(14), pp. 7150–7158. doi: 10.1021/ac502040v.

Mehdiani, A. *et al.* (2015) 'An Innovative Method for Exosome Quantification and Size Measurement', *Journal of Visualized Experiments*, (95), pp. 1–9. doi: 10.3791/50974.

Minagar, A. *et al.* (2002) 'The role of macrophage/microglia and astrocytes in the pathogenesis of three neurologic disorders: HIV-associated dementia, Alzheimer disease, and multiple sclerosis', *Journal of the Neurological Sciences*. Elsevier, 202(1–2), pp. 13–23. doi: 10.1016/S0022-510X(02)00207-1.

Miyamoto, A. *et al.* (2016) 'Microglia contact induces synapse formation in developing somatosensory cortex', *Nature Communications*. The Author(s), 7, p. 12540. Available at: <http://dx.doi.org/10.1038/ncomms12540>.

Muffat, J. *et al.* (2015) 'Efficient derivation of microglia-like cells from human pluripotent stem cells', 27(4), pp. 329–336. doi: 10.1111/j.1525-1446.2010.00862.x.Asthma.

Mulcahy, L. A., Pink, R. C. and Carter, D. R. F. (2014) 'Routes and mechanisms of extracellular vesicle uptake', *Journal of Extracellular Vesicles*, 3(1), pp. 1–14. doi: 10.3402/jev.v3.24641.

Nadjar, A. (2018) 'Role of metabolic programming in the modulation of microglia phagocytosis by lipids', *Prostaglandins Leukotrienes and Essential Fatty Acids*. Elsevier Ltd, 135(July), pp. 63–73. doi: 10.1016/j.plefa.2018.07.006.

Naj, A. C. *et al.* (2011) 'Common variants at MS4A4/MS4A6E, CD2AP, CD33 and EPHA1 are associated with late-onset Alzheimer's disease', *Nature Genetics*. Nature Publishing Group, a division of Macmillan Publishers Limited. All Rights Reserved., 43, p. 436. Available at: <http://dx.doi.org/10.1038/ng.801>.

Ostasiewicz, P. *et al.* (2010) 'Proteome, phosphoproteome, and N-glycoproteome are quantitatively preserved in formalin-fixed paraffin-embedded tissue and analyzable by high-resolution mass spectrometry', *Journal of Proteome Research*, 9(7), pp. 3688–3700. doi: 10.1021/pr100234w.

Paloneva, J. *et al.* (2002) 'Mutations in two genes encoding different subunits of a receptor signaling complex result in an identical disease phenotype', *American Journal of Human Genetics*, 71, pp. 656–662. doi: 10.1086/342259.

Parkhurst, C. N. *et al.* (2013) 'Microglia Promote Learning-Dependent Synapse Formation through Brain-Derived Neurotrophic Factor', *Cell*. Cell Press, 155(7), pp. 1596–1609. doi: 10.1016/J.CELL.2013.11.030.

Pascua-Maestro, R. *et al.* (2019) 'Extracellular Vesicles Secreted by Astroglial Cells Transport Apolipoprotein D to Neurons and Mediate Neuronal Survival Upon Oxidative Stress', *Frontiers in*

Cellular Neuroscience, 12(January), pp. 1–13. doi: 10.3389/fncel.2018.00526.

Penzes, P. *et al.* (2011) 'Dendritic spine pathology in neuropsychiatric disorders', *Nature Neuroscience*. Nature Publishing Group, a division of Macmillan Publishers Limited. All Rights Reserved., 14, p. 285. Available at: <http://dx.doi.org/10.1038/nn.2741>.

Piers, T. M. *et al.* (2020) 'A locked immunometabolic switch underlies TREM2 R47H loss of function in human iPSC--derived microglia', *FASEB journal : official publication of the Federation of American Societies for Experimental Biology*, 34, pp. 2436–2450. doi: 10.1101/766089.

Qu, Y. *et al.* (2007) 'Nonclassical IL-1 Secretion Stimulated by P2X7 Receptors Is Dependent on Inflammasome Activation and Correlated with Exosome Release in Murine Macrophages', *The Journal of Immunology*, 179(3), pp. 1913–1925. doi: 10.4049/jimmunol.179.3.1913.

Schiera, G., Di Liegro, C. M. and Di Liegro, I. (2015) 'Extracellular Membrane Vesicles as Vehicles for Brain Cell-to-Cell Interactions in Physiological as well as Pathological Conditions', *BioMed Research International*. Hindawi Publishing Corporation, 2015. doi: 10.1155/2015/152926.

Schneider, D. J. *et al.* (2017) 'Mechanisms and modulation of microvesicle uptake in a model of alveolar cell communication', *Journal of Biological Chemistry*, 292(51), pp. 20897–20910. doi: 10.1074/jbc.M117.792416.

Shirotani, K. *et al.* (2019) 'Aminophospholipids are signal-transducing TREM2 ligands on apoptotic cells', *Scientific Reports*. Springer US, 9(1), pp. 1–9. doi: 10.1038/s41598-019-43535-6.

Takahashi, K., Rochford, C. D. P. and Neumann, H. (2005) 'Clearance of apoptotic neurons without inflammation by microglial triggering receptor expressed on myeloid cells-2', *The Journal of Experimental Medicine*, 201(4), pp. 647–657. doi: 10.1084/jem.20041611.

Ulland, T. K. *et al.* (2017) 'TREM2 Maintains Microglial Metabolic Fitness in Alzheimer's Disease', *Cell*. Elsevier Inc., 170(4), pp. 649-663.e13. doi: 10.1016/j.cell.2017.07.023.

Wang, Y. *et al.* (2015) 'TREM2 lipid sensing sustains microglia response in an Alzheimer's disease model', *Cell*, 160(6), pp. 1061–1071. doi: 10.1016/j.cell.2015.01.049.TREM2.

Wesén, E. *et al.* (2017) 'Endocytic uptake of monomeric amyloid- β peptides is clathrin- A nd dynamin-independent and results in selective accumulation of A β (1-42) compared to A β (1-40)', *Scientific Reports*, 7(1), pp. 1–14. doi: 10.1038/s41598-017-02227-9.

Witwer, K. W. *et al.* (2013) 'Standardization of sample collection, isolation and analysis methods in extracellular vesicle research', *Journal of Extracellular Vesicles*, 2(1), pp. 1–29. doi: 10.3402/jev.v2i0.20360.

Xiang, X. *et al.* (2018) 'The Trem2 R47H Alzheimer's risk variant impairs splicing and reduces Trem2 mRNA and protein in mice but not in humans', *Molecular Neurodegeneration*. Molecular Neurodegeneration, 13(1), pp. 1–14. doi: 10.1186/s13024-018-0280-6.

Yang, Y. *et al.* (2018) 'Inflammation leads to distinct populations of extracellular vesicles from

microglia', *Journal of Neuroinflammation*. *Journal of Neuroinflammation*, 15(1), p. 168. doi: 10.1186/s12974-018-1204-7.

Zhang, B. *et al.* (2013) 'Integrated Systems Approach Identifies Genetic Nodes and Networks in Late-Onset Alzheimer's Disease', *Cell*. Elsevier, 153(3), pp. 707–720. doi: 10.1016/j.cell.2013.03.030.

Zhong, L. *et al.* (2017) 'TREM2/DAP12 complex regulates inflammatory responses in Microglia via the JNK signaling pathway', *Frontiers in Aging Neuroscience*, 9(JUN), pp. 1–9. doi: 10.3389/fnagi.2017.00204.

Zou, W. *et al.* (2019) 'Exosome Release Is Regulated by mTORC1', *Advanced Science*, 6(3), pp. 1–12. doi: 10.1002/advs.201801313.

Figure legends

Figure 1 – Exosome characterisation

Western blot of exosomes extracted from common variant (Cv) and R47H^{het} TREM2 expressing iPS-Mg express the exosomal markers CD63, and CD9, with exosomes extracted from human serum used as a positive control (Exo standard) (**A**). The extracted exosomal fraction did not contain calnexin, indicating that the fraction is clear of ER contamination, whilst the exosome fraction contained another exosomal marker CD81 (**B**). Size distribution curves of exosomes from Cv and R47H^{het} iPS-Mg, against a human CSF standard assessed by nanoparticle tracking analysis (NTA) (**C**, **D**). Quantification of the exosome concentration of Cv or R47H^{het} iPS-Mg derived exosomes following NTA (**E**) or by western blot of CD63 expression (**F**). The full blots for A and B can be found in Supplementary Fig 5 and expanded datasets for D-F in Supplementary Fig 4. All data are the mean ± SEM, n ≥ 4 with one-way ANOVA (**D**) and Students *t*-test (**E** and **F**) * $\rho < 0.05$, *** $\rho < 0.001$.

Figure 2 – Exosome secretion can be rescued

Western blot of exosomal CD63 levels, (used to approximate exosome secretion), following stimulation of iPS-Mg with 100 ng/ml LPS or apoptotic neurons (ratio of 2 apoptotic neurons: 1 iPS-Mg) for 24 h (**A**) and quantification of CD63 expression (**B**). Western blot of exosomal CD63 (**C**) and CD63 quantification (**D**) following exposure of iPS-Mg to 10 mM cyclocreatine for 24 h. The full blots for A and C can be found in Supplementary Fig 5 and expanded datasets for B and D in Supplementary Fig 4. Data are the mean ± SEM, n ≥ 3 following two-way ANOVA followed by Tukey's post-hoc tests, n.s not significant, * $\rho < 0.05$, ** $\rho < 0.01$.

Figure 3 – Proteomics of exosomes

Mass spectrometry was performed on exosomes extracted from iPS-Mg. Over 70% of the proteins detected by mass spectrometry (blue) have been previously linked to exosomal proteins (**A**). 2147 proteins have been previously published in a meta-analysis of high-throughput proteomics of exosomes (Choi *et al.*, 2013), whilst 475 proteins were shared with the online repository of exosomal proteins (ExoCarta-Accession, red). This was also verified following analysis of the proteins for their cellular

compartment of origin (**B**). The proteins are significantly associated with exosomes, followed by the lysosomes and cytoplasm relative to the annotated control genome. This confirms the extracted particles to be exosomes. The difference between exosomes secreted from Cv and R47H^{het} iPS-Mg was compared by volcano plot (**C**). The ratio in abundance of proteins in R47H exosomes, compared with Cv exosomes, was plotted in the x-axis whilst the significance of the change, in form of the ρ value, was plotted in the y-axis, meaning that any proteins in the top left and right section had a significant 2-fold change. Nine proteins were found to be significantly packaged into exosomes originating from R47H^{het} iPS-Mg compared with exosomes from Cv iPS-Mg (**C**). The function of these proteins was analysed through STRING analysis (**D**), which indicated that some of the proteins increasingly packaged into R47H^{het} exosomes are involved in the negative regulation of transcription and metabolic processes, $n = 3$ independent experiments. Heatmap of the analysis of microglial gene signature in all iPS-Mg lines and clones used in this study using a custom gene array (**E**).

Figure 4 – Stimulation-induced differential changes in exosomal proteins following TLR4 stimulation

Volcano plots of the effect of LPS stimulation on exosomal proteins in Cv iPS-Mg (**A**) and R47H^{het} iPS-Mg (**B**). Proteins of interest were circled and further plotted (**C**). Data are mean \pm SEM with $n = 3$ independent experiments. Two-way ANOVA followed by Tukey's post-hoc test with * $\rho < 0.05$, ** $\rho < 0.01$.

Figure 5 – Changes in exosomal protein following TREM2 ligand exposure

Volcano plots for the effect of apoptotic neuron treatment on exosomal proteins in Cv iPS-Mg (**A**) and R47H^{het} iPS-Mg (**B**). Proteins of interest were further plotted (**C**). Data are mean \pm SEM with $n = 3$ independent experiments. Two-way ANOVA followed by Tukey's post-hoc test with * $\rho < 0.05$, ** $\rho < 0.01$.

Figure 6 – Comparison of exosomal proteins increased following exposure to a TREM2 ligand

Volcano plots comparing the increased abundance levels of exosomal proteins from Cv or R47H^{het} iPS-Mg treated with apoptotic neurons to stimulate TREM2-mediated pathways. (**A**). Abundance levels of some of the proteins observed to change following this stimulation (**B**). Data are mean \pm SEM with $n = 3$. Two-way ANOVA followed by Tukey's post-hoc test with * $\rho < 0.05$, ** $\rho < 0.01$.

Figure 7 – Uptake of iPS-Mg exosomes into SH-SY5Y

iPS-Mg derived exosomes were added to differentiated SH-SY5Y (**workflow: A**). Uptake of exosomes into SH-SY5Y was determined by imaging DiO-labelled exosomes inside SH-SY5Y, (the latter were stained with BioTracker 555 Orange Cytoplasmic Membrane Dye, 2 $\mu\text{g/ml}$) after 1h and 24 h of incubation with the exosomes (**B**) Scale bar = 10 μm . Uptake was quantified by FACs analysis of DiI-labelled exosomes and compared with unstained cells (Unst), (**C**) or with DiI-labelled PBS as a negative control (PBS) or following 30 min preincubation with cytochalasin D (CytoD, 10 μM), chlorpromazine (CPZ, 5 $\mu\text{g/ml}$) or genistein (200 μM) (**D**). Expanded dataset for D can be found in Supplementary Fig

4. Data are the mean \pm SEM with one-way ANOVA followed by Tukey's post-hoc test, $n \geq 4$. ** $p < 0.01$, * $p < 0.05$, ns, not significant.

Figure 8 – SH-SY5Y viability following exosome incubation

The effect of exosomes on the viability of SH-SY5Y assessed with prodidium iodide (PI) staining and FACS analysis. Baseline cell death following addition of exosomes from unstimulated iPS-Mg from Cv or R47H^{het} to SH-SY5Y (**A** and **B**). Cell death in SH-SY5Y challenged with H₂O₂ (100 μ M) for 24 h in the presence of exosomes from Cv or R47H^{het} iPS-Mg or (**C** and **D**). Expanded datasets for B and D can be found in Supplementary Fig 4. One-way ANOVA followed by Tukey's post-hoc test, with $n \geq 5$ and $n \geq 4$ for **B** and **D** respectively, ** $p < 0.01$.

Video 1. Representative video of NTA showing particles in the exosomal fraction of iPS-Mg.

Video 2. Representative video of NTA showing no particles in the cell medium itself.

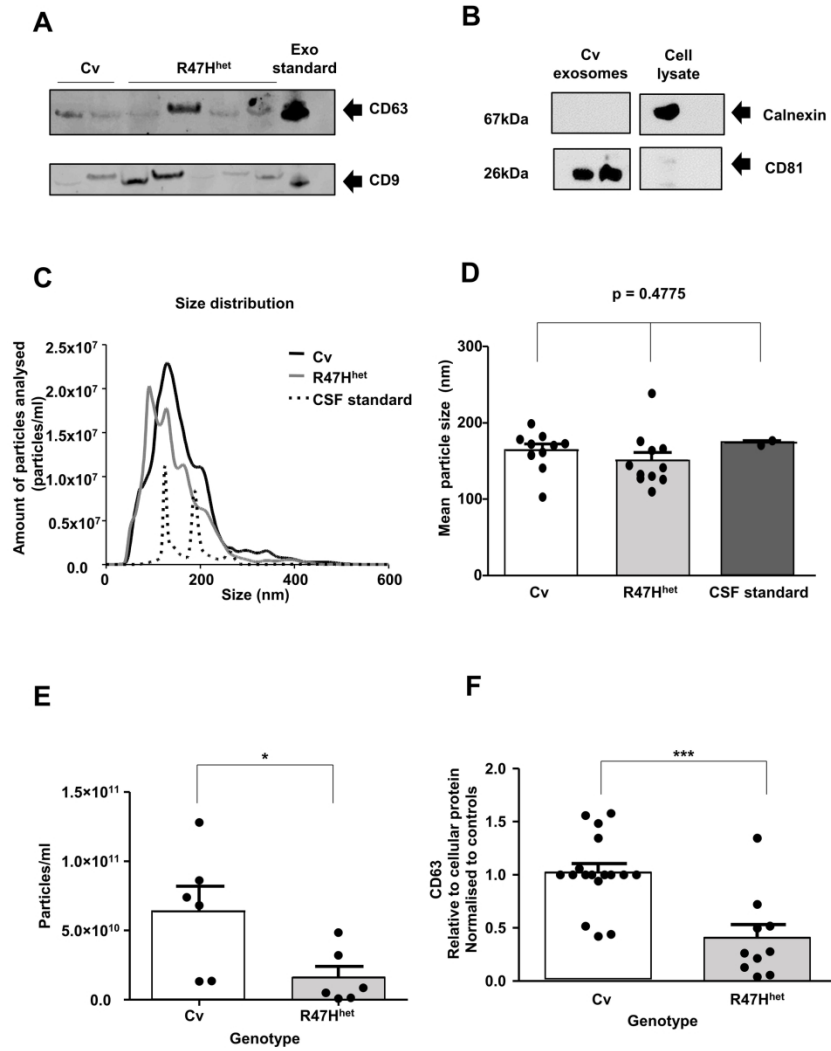


Figure 1

190x275mm (300 x 300 DPI)

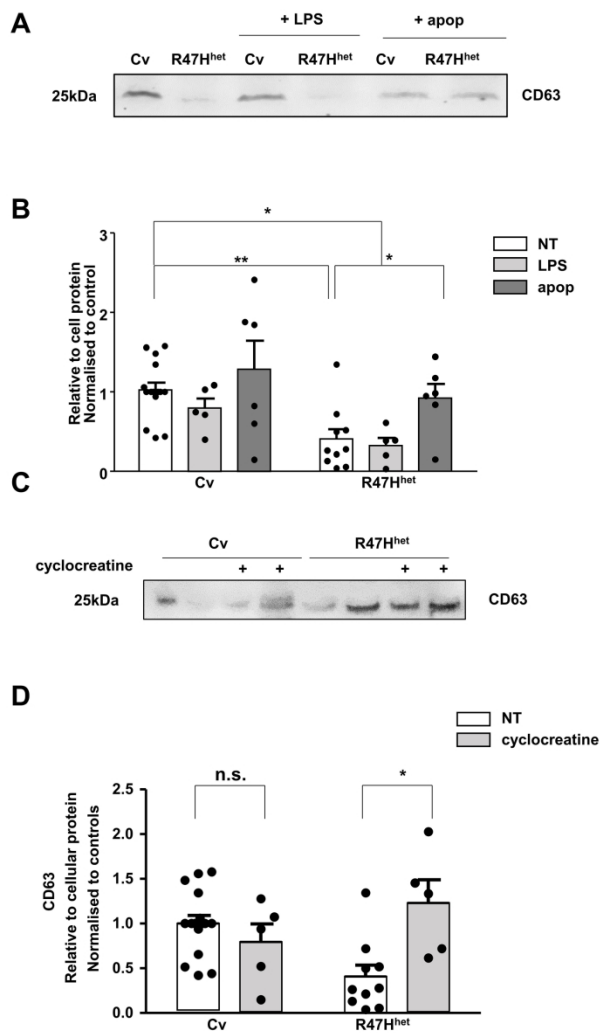


Figure 2

190x275mm (300 x 300 DPI)

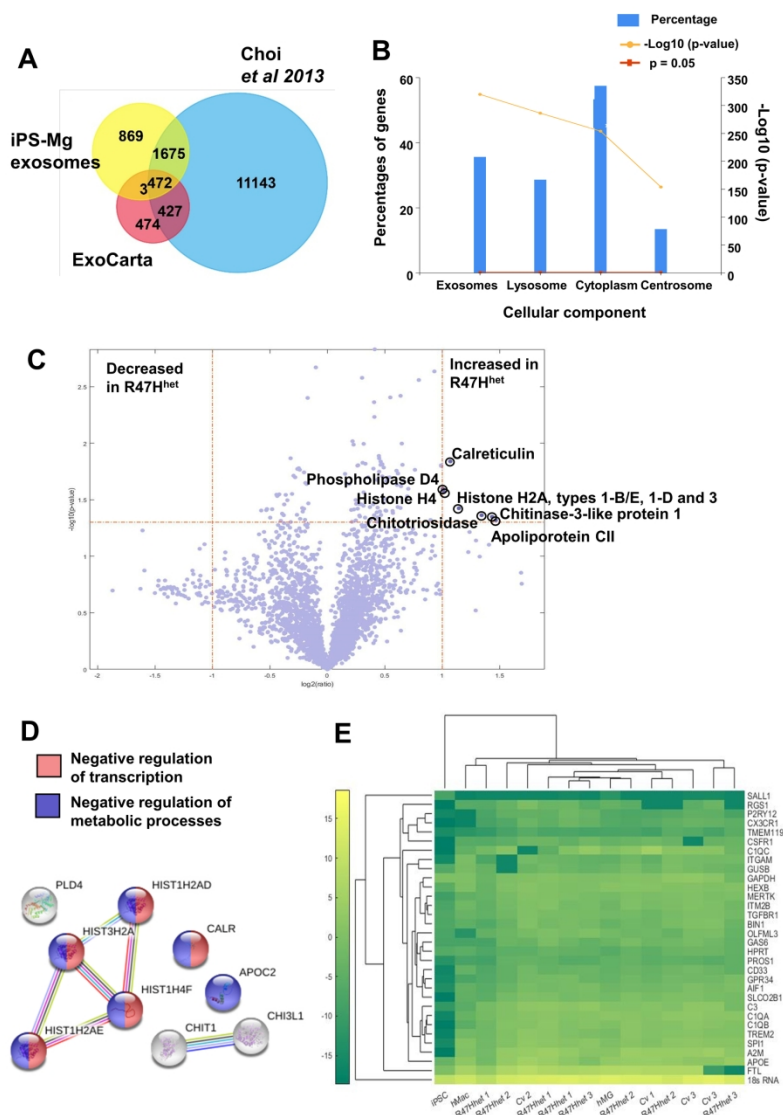


Figure 3

190x275mm (300 x 300 DPI)

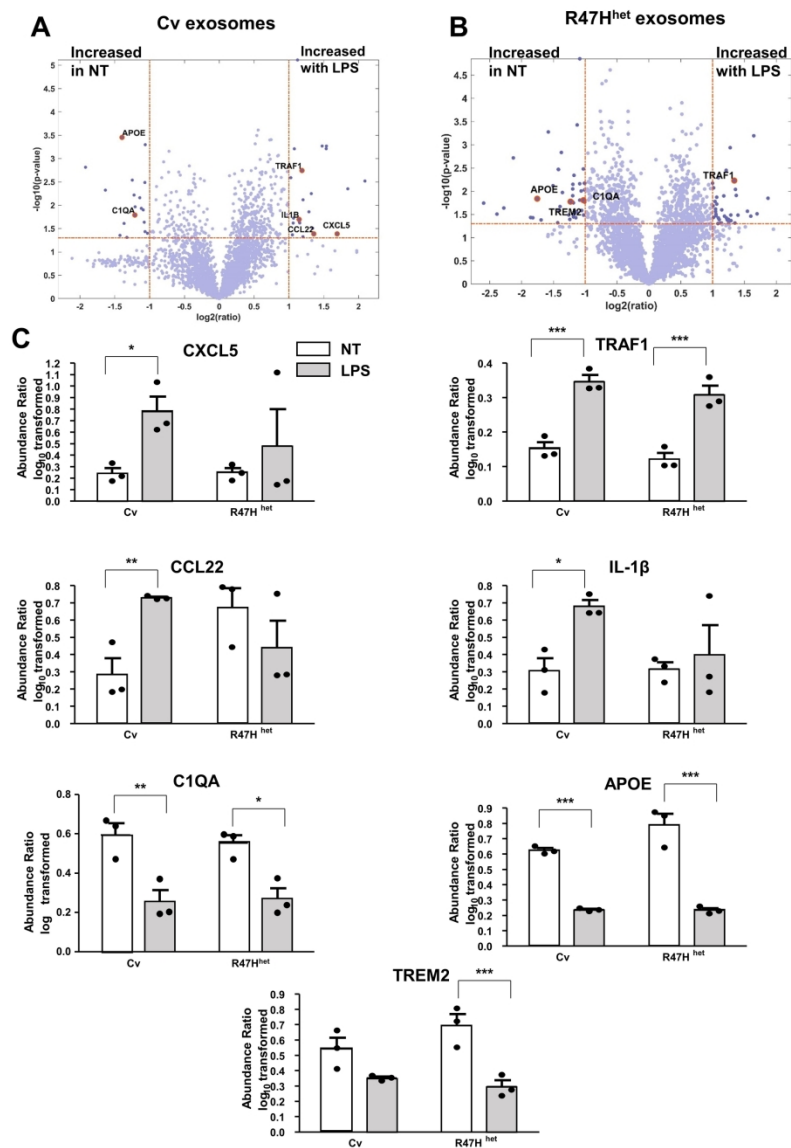


Figure 4

190x275mm (300 x 300 DPI)

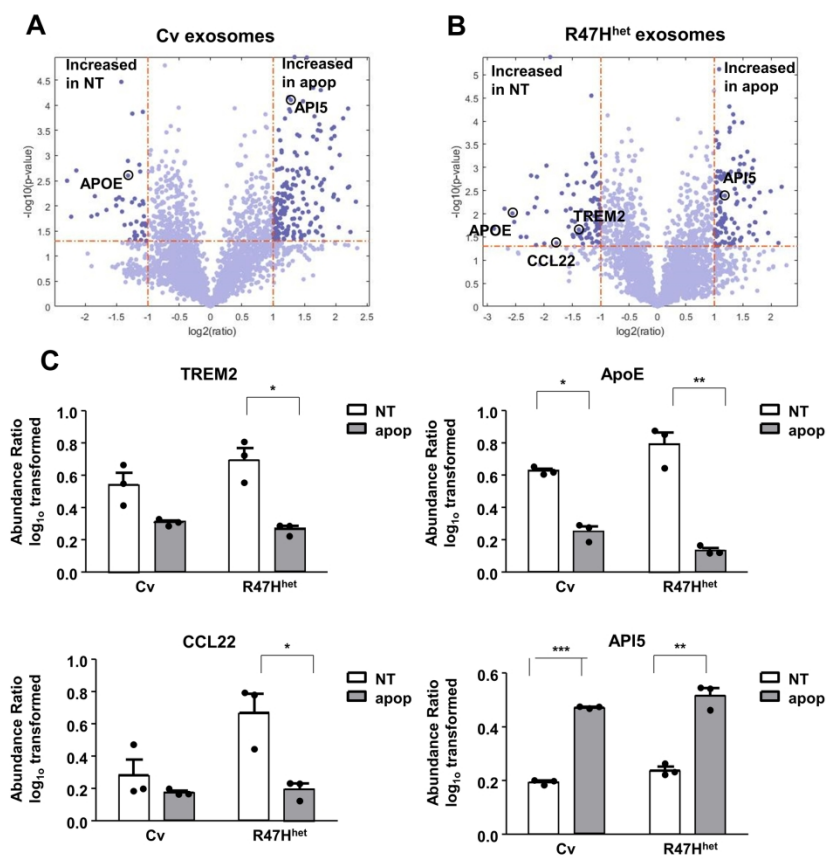


Figure 5

190x275mm (300 x 300 DPI)

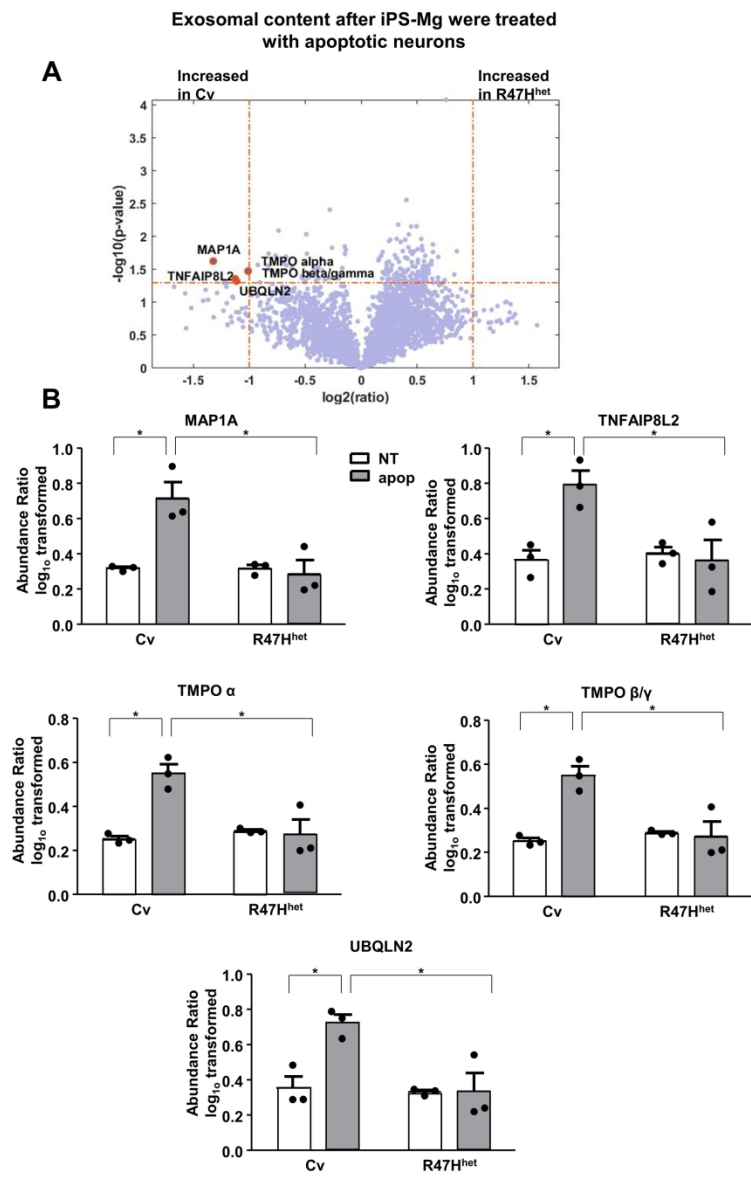


Figure 6

190x275mm (300 x 300 DPI)

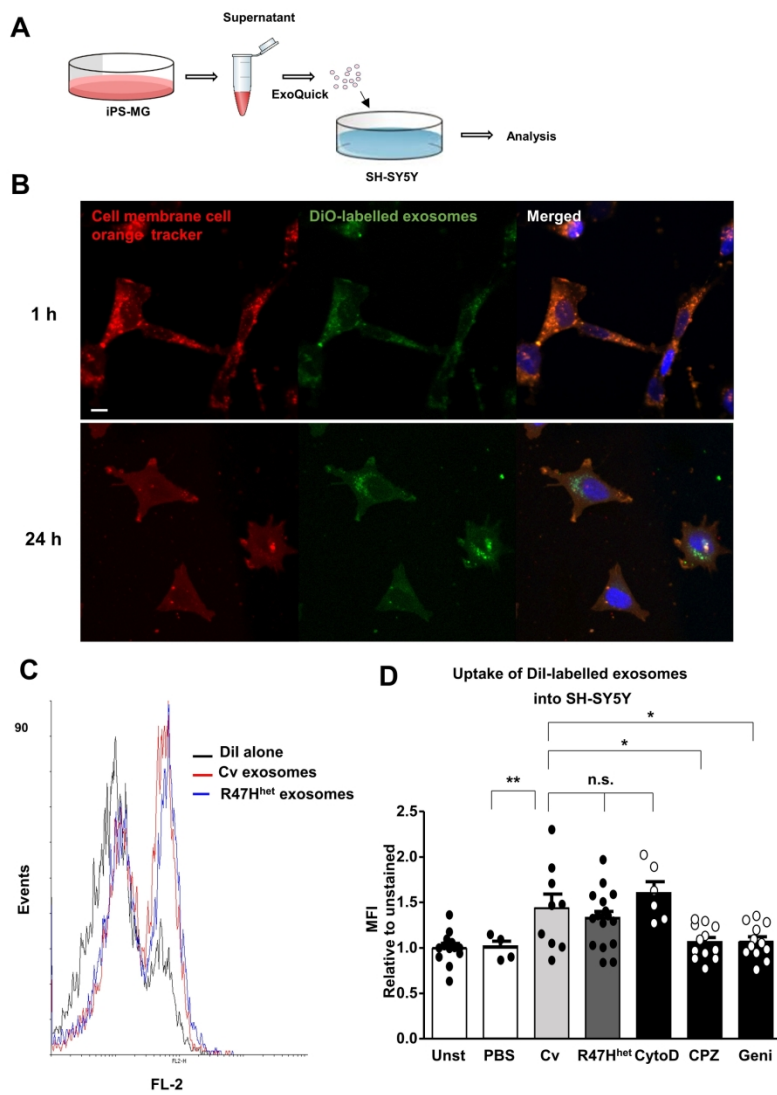


Figure 7

190x275mm (300 x 300 DPI)

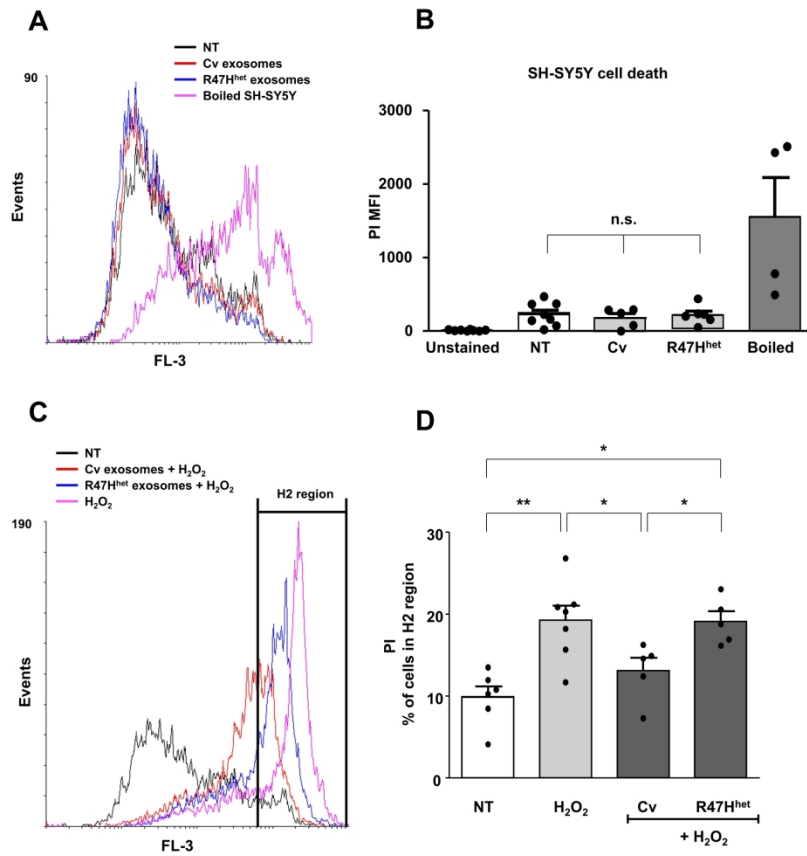


Figure 8

190x275mm (300 x 300 DPI)

50 word summary

Mallach *et al.* investigated the effect of the R47H *TREM2* variant in human induced pluripotent stem cell microglia-derived cells on exosome secretion and content. They found decreased exosome secretion rate from *TREM2* variants, linked to decreased energy availability, and differences in exosomal protein content, which influenced the viability of neuron-like cells.

